JAAS

ROYAL SOCIETY OF CHEMISTRY

PAPER

View Article Online
View Journal | View Issue

Cite this: J. Anal. At. Spectrom., 2024, 39, 1903

Quantitative depth profile analysis using short single pulse responses in LA-ICP-Q-MS experiments†

Maximilian Podsednik,[ab] Florian Fahrnberger,[a] David Ken Gibbs,[a] Birgit Achleitner,[a] Silvia Larisegger,[b] Michael Nelhiebel,[c] Herbert Hutter[a] and Andreas Limbeck *[a]

The demand for high-resolution imaging, and high sample throughputs in LA-ICP-MS experiments has led to developing rapid-response ablation cells with low dispersion. These cells can achieve short transient signals called single pulse responses (SPRs), whose width is in the single-digit millisecond range at 1% of the maximum. However, coupled with ICP-Q-MS, recording those short signals poses a problem due to the sequential measurement of selected *m*/*z* ratios. If more than one *m*/*z* ratio is targeted, the time resolution of quadrupole detection systems is insufficient for accurately determining short SPRs. This work focuses on utilizing rapid response ablation cells for the analysis of multiple elements with quadrupole-based detection systems in the SPR mode. To achieve this, an ArF-excimer laser equipped with a rapid-response ablation chamber is coupled to an ICP-MS with a short settling time of 0.2 ms and below. The two naturally occurring Ag-isotopes were analyzed in the NIST SRM 612 to optimize the dwell times for ideal data acquisition. The data shows that the ratio of the dwell time and the settling time, plays a crucial role. With the optimized parameters, the natural ratio of ^{107}Ag and ^{109}Ag within a 10 ms FW0.01M transient signal could be determined. This concept of LA-ICP-MS was then applied for depth profiling analysis of Al-doped SiC, a wide bandgap semiconductor. This procedure acquired depth profiles on 30 different sample locations in approximately 2 minutes with an exceptional depth resolution of 55 nm.

Received 13th March 2024
Accepted 17th May 2024

DOI: 10.1039/d4ja00082j

rsc.li/jaas

1 Introduction

LA-ICP-MS has gained popularity in many different fields, like biology,[1,2] geology,[3,4] and material science,[5,6] for the analysis of solid samples, due to its high dynamic range, low limits of detections, and high sample throughput.[7,8] Moreover, LA-ICP-MS is commonly used for imaging and depth profiling experiments.[9–11] Nonetheless, this technique's sensitivity and maximum scan speed are primarily limited by the washout time of the ablated material. As a result, rapid response ablation cells with low dispersion have been developed to attain short transient signals, known as single pulse responses (SPR), whose widths are in the single-digit millisecond range at FW0.01M.[12–14] The aerosol transport systems have also been updated to keep up with the fast washout behavior of rapid response ablation cells. This was achieved by using tubing with a smaller inner diameter and eliminating dead volumes in the injector of the ICP torch. As demonstrated by previous studies, these enhancements result in higher sensitivity, better resolution, and higher sample throughput for LA-ICP-MS experiments.[15]

To fully utilize the advantage of rapid response ablation cells for multielement analysis, they are coupled to ICP-ToF-MS since their fast acquisition rate of a whole *m*/*z*-spectra allows the recording of short SPRs with the required time resolution.[16] In contrast, the more frequently applied quadrupole-based ICP-MS systems (single-quadrupole and triple quadrupole instrumentation) offer enhanced sensitivity, with the drawback of measuring the *m*/*z* ratios of interest sequentially. Thus, for multi-element analysis switching between the respective isotopes is necessary. Therefore, a time interval is needed to adjust and stabilize the voltages in the quadrupole, which is called settling time, a factor usually predefined by the instrument manufacturer.[17] Therefore, each measurement cycle, or duty cycle, consists of the sum of the settling time and the dwell time multiplied by the number of measured *m*/*z* ratios.[18] While the dwell time of most ICP-MS can be reduced to 0.1 ms and below, the settling time of most commercially available

[a]TU Wien, Institute of Chemical Technologies and Analytics, Getreidemarkt 9/164-I^{2}AC, 1060 Vienna, Austria. E-mail: andreas.limbeck@tuwien.ac.at
[b]KAI Kompetenzzentrum Automobil- und Industrieelektronik GmbH, Argentinierstraße 8, 1040 Wien, Austria
[c]KAI Kompetenzzentrum Automobil- und Industrieelektronik GmbH, Technologiepark Villach Europastraße 8, 9524 Villach, Austria

† Electronic supplementary information (ESI) available. See DOI: https://doi.org/10.1039/d4ja00082j

instruments is usually in the range of 1–2 ms. This demonstrates the quadrupole-based mass analyzer's limitation in handling SPR signals of rapid response ablation cells. Considering the measurement of two isotopes with a dwell time of 0.5 ms and a settling time of 2.0 ms, the duty cycle of the experiment would be 5 ms, resulting in three data points per isotope for a 15 ms SPR. Moreover, the ratio of the dwell time and the settling time needs to be considered, known as the integration ratio. High integration ratios are favored since no data recording occurs during the settling time, leading to a huge loss of information. The example also represents this since only 20% of the SPR duration would be used for analysis of the selected isotopes.

Thus, different measurement strategies are required to employ these rapid response ablation cells with low aerosol dispersion when coupled to quadrupole instruments. For this purpose, the concept of overlapping laser shots, or dosage, has been introduced by Šala *et al.*[19] to improve the image quality of quadrupole-based multi-element experiments. The concept of dosage has further been used by Willner *et al.*[5] for depth profiling to achieve sufficient sensitivity for the analysis of S in polymers. However, compared to methods based on SPR analysis, longer measurement times are required for the same sample area and transport efficiency, or plasma load could also be affected by the increased amount of ablated sample material. Moreover, especially for depth profiling, the concept of dosage results in a decreased depth resolution.

To utilize rapid response ablation cells at their full potential when coupled to ICP-QMS, the problem of handling short SPR in LA-ICP-QMS experiments is tackled in this work. For this purpose, the "NexION5000" ICP-MS is utilized, providing a settling time of 0.2 ms coupled to the "imageGEO193" an ArF-excimer laser equipped with a rapid response ablation chamber. The goal of this work was to achieve the required time resolution with a quadrupole detection system for the measurement of short SPRs for multiple elements. The applicability was further demonstrated for depth profile analysis in Al-doped SiC, and the results are compared to time of flight-secondary ion mass spectrometry (ToF-SIMS), which belongs together with glow discharge-optical emission spectroscopy or mass spectrometry (GD-OES/MS) and X-ray photoelectron spectroscopy (XPS) to the commonly applied techniques for depth profile analysis.[20]

2 Experimental

2.1 Samples

All measurements were conducted on NIST SRM 612 (National Institute of Standards and Technology, USA) and four different SiC samples locally implanted with Al. The samples have a constant Al implantation for the upper 250 nm with different Al concentrations: 3×10^{20} cm^{-3}, 1×10^{20} cm^{-3}, 3×10^{19} cm^{-3}, and 1×10^{19} cm^{-3}.

2.2 Instrumentation

2.2.1 LA ICP MS. For the LA-ICP-MS measurements, the ImageGEO193 (Elemental Scientific Laser, USA), an ArF excimer laser with a wavelength of 193 nm, a pulse width of 7 ns and a flat-top beam profile, was used. The laser is equipped with the "TwoVol3", a rapid-response ablation cell. A PEEK capillary (ID: 1.0 mm) and a dual concentric injector (DCI) have been used as an aerosol transport system. A NexION5000 ICP-MS (PerkinElmer, USA) was used as a detection system in standard mode. Before all experiments, the ICP-MS was tuned for maximum intensity of the 115In signal and ThO+/Th+ ratio below 3% with the NIST SRM 612. The data was recorded using the instrument software SyngistixTM (Version: 3.5), and iolite v4 (Version: v4.8.9) was used for the evaluation. The ICP-MS and laser parameters can be seen in Table 1.

2.2.2 ToF-SIMS. ToF-SIMS depth profiles were performed on a TOF.SIMS5 (ION-TOF, Germany) instrument as a reference measurement. For the analysis, 25 keV Bi^+ primary ions were used in the high mass resolution operational mode "high current bunched". An area of 100 μm × 100 μm was investigated using a raster of 128 × 128 pixels. In this experiment, positive ions were analyzed; therefore, the depth profiles were conducted using 2 keV O_2^+ ions (300 μm × 300 μm). To compensate for surface charges, a low-energy electron flood gun (20 V) was used.

3 Results and discussion

3.1 Dwell time optimization for handling short SPRs with quadrupole detection systems

Accurately measuring short transient signals with ICP-MS requires recording sufficient data points for each isotope of interest within the washout time of the ablated material. Thus, when using ICP-MS instrumentation based on quadrupole detectors, the optimization of the duty cycle is crucial for

Table 1 ICP-MS and laser parameters for the LA-ICP-MS measurement

ICP-MS detection system		
RF power		1600 W
Nebulizer gas flow		0.98 l min^{-1}
Cool gas flow		16 l min^{-1}
Auxiliary gas flow		1.2 l min^{-1}
Experiment	**NIST SRM 612**	**Al-doped SiC**
Measured isotopes	^{107}Ag, ^{109}Ag	^{27}Al, ^{29}Si
Dwell time	0.1 ms, 0.3 ms, 0.5 ms, 0.7 ms, 0.9 ms, 1.1 ms, 1.3 ms, 1.5 ms, 2.0 ms	0.3 ms
Settling time	0.2 ms	0.2 ms
ImageGEO^{193}		
Laser fluence		3.5 J cm^{-2}
Spot size		20 × 20 μm
Scan speed		0.5 mm s^{-1}
Repetition rate		20 Hz
Chamber He flow		450 ml min^{-1}
Sniffer He flow		500 ml min^{-1}

reliable data recording. Therefore, a systematic investigation of the effect of the duty cycle on data acquisition was performed. For this purpose, the NIST SRM 612 was used, particularly the two naturally occurring Ag isotopes (^{107}Ag and ^{109}Ag). The analysis of the Ag-isotopes was chosen since both isotopes have an almost 50 : 50 natural abundance. Therefore, an almost identical signal sequence should be achieved if the optimization of the dwell time is successful.

To establish a defined washout time of the ablated NIST SRM 612, the He carrier flow of the chamber and the sniffer gas flow were adjusted (see Chapter 2.2.1), resulting in a reproducible washout time of 10 ms at FW0.01M for both Ag isotopes. To evaluate the impact of the dwell time's length on the quality of the data recording, nine different dwell times ranging from 0.1 ms to 2.0 ms were investigated. Considering a constant settling time of 0.2 ms, this results in duty cycles between 0.6 ms and 4.4 ms for the measurement of the two Ag isotopes. For each duty cycle, the NIST SRM 612 was ablated using line scans with 30 not overlapping ablation areas, resulting in 30 baseline separated SPRs per measurement. Exemplarily, the ^{107}Ag and ^{109}Ag SPRs can be seen in Fig. 1 for two different measurements using a duty cycle of 1.0 ms (a) and 3.4 ms (b).

In Fig. 1, one can see that (subjective) a good accordance of the signals recorded for the two Ag isotopes was achieved using a 1.0 ms duty cycle for the analysis. On the other hand, for the measurement with a 3.4 ms duty cycle (subjective) a visible difference between the ^{107}Ag and the ^{109}Ag signal becomes noticeable. Moreover, due to the prolonged dwell time, fewer data points are recorded, resulting in the smoothening of the signal. As a result, the time resolution for longer duty cycles is insufficient for accurately determining the exact peak maxima of both isotopes. For a more detailed discussion, the average signal intensity of the peak maxima for each duty cycle is examined in Fig. 3 to get an overview of the whole measurement series. For this comparison, the counts per second signals were used to compensate for the variation in signal intensity due to the different recording times per duty cycle.

As expected, the mean I_{max} is decreasing with increasing dwell times and, thus, duty cycle times. This can be attributed to the simultaneous recording of the peak maxima and the declining and rising parts of the SPR within one data point. Looking at the relative standard deviation of the mean I_{max}, a variation between 20% and 30% can be seen; considering that only one data point of the short signal is used, this result already demonstrates the reproducibility of this approach. One thing worth mentioning is that the shortest duty cycle of 0.6 ms shows the highest relative standard deviation, while a duty cycle of 1.0 ms exhibits the smallest. The low integration ratio is expected to be responsible for that result.

To overcome the problems associated with adequate detection of the peak maxima, in the next step, background corrected peak areas have been determined and are compared for the different duty cycles (see Fig. 3).

In contrast to the averaged peak maxima, the peak area analysis of the averaged signal does not show significant changes with increasing dwell times. Moreover, the overall RSD of the peak area is lower and ranges between 12% and 20%, with rising deviations for higher duty cycles. However, to determine the impact of the length of the duty cycle on an individual SPR, which is a prerequisite for spatially resolved analysis, looking at the maximum peak intensity and the peak area is not sufficient. Therefore, the ^{107}Ag/^{109}Ag ratio is examined for each individual SPR, and the 30 ratios are averaged for each investigated duty cycle. The result can be seen in Fig. 4 for the different duty cycles.

Like the comparison of the peak area, the averaged ^{107}Ag/^{109}Ag ratio shows no significant variation. However, analyzing the relative standard deviation indicates a minimum of 13% for a duty cycle of 1.0 ms, which constantly increases to 37% for the most extended duty cycle. In this case, the relative standard deviation reflects the discrepancy of the individual single pulse response.

To conclude, although the higher duty cycles have the best integration ratio, their time resolution is insufficient to describe the short transient signals for multiple isotopes adequately. This is in accordance with the initial observation of the raw data (*cf.* Fig. 2). On the other hand, the lowest duty cycle of 0.6 ms holds an integration ratio below 50%. Therefore, a duty cycle of 1.0 ms represents an ideal compromise of maximizing time resolution while reducing information loss, reflected by the lowest standard deviation of the isotope ratios.

3.2 Multi-element depth profiles of Al-doped SiC using SPRs with a quadrupole detection system

The proposed concept of LA-ICP-MS utilizing SPRs in combination with a quadrupole-based mass analyzer was applied for

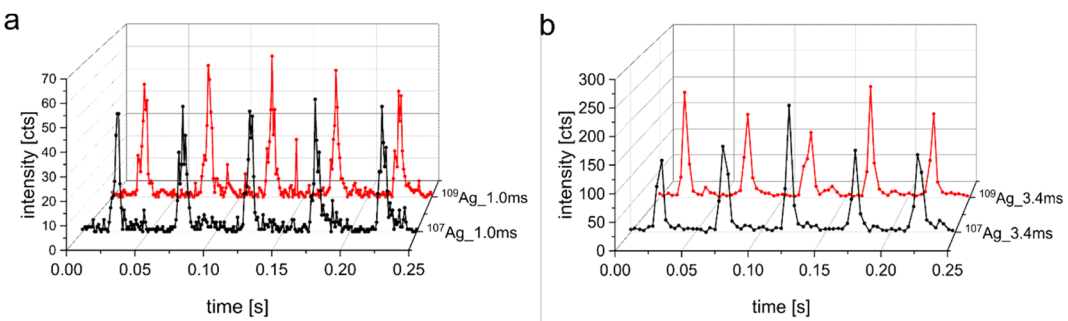

Fig. 1 Comparison of the SPRs of the Ag isotopes recorded with duty cycles of 1.0 ms (a) and 3.4 ms (b).

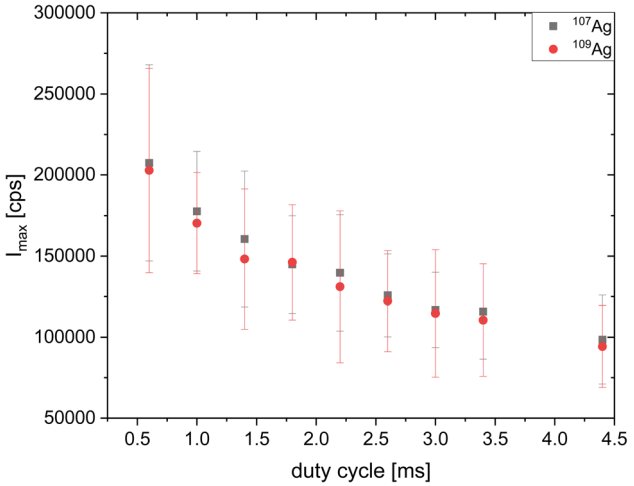

Fig. 2 Averaged maximal intensity value of the ^{107}Ag and ^{109}Ag SPRs (n = 30) for different duty cycles. The depicted error bars represent the standard deviation of the 30 measured peak maxima.

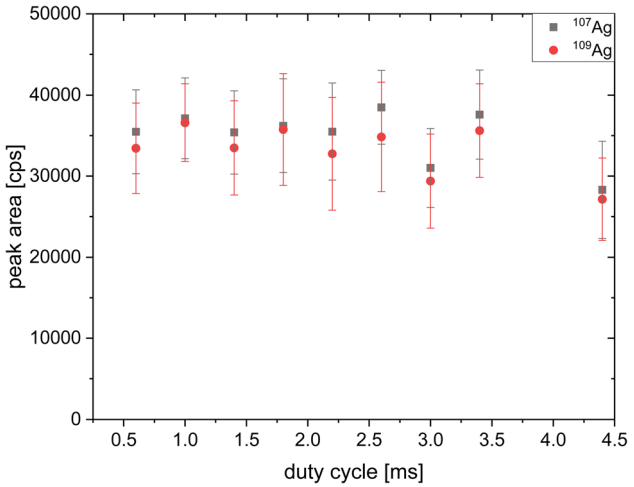

Fig. 3 Mean background corrected peak area of the recorded SPRs (n = 30) of ^{107}Ag and ^{109}Ag with different duty cycles. Depicted error bars correspond to the standard deviation of the 30 measured peak areas.

depth profile measurements in the wide band gap material SiC, which is decisive for more efficient power devices.[21,22] One crucial factor for the functionality of semiconductor devices is the distribution and concentration of dopants[23,24] within the sample. Therefore, analytical methods, which offer high sensitivity, lateral resolution, and high sample throughput, are mandatory to optimize manufacturing and implantation processes. To demonstrate the applicability and advantages of the developed procedure, the depth distribution of Al, a p-type dopant,[25] in SiC is analyzed.

For this purpose, the instrumental parameters obtained in the previously mentioned NIST SRM 612 experiments have been applied. In these measurements, a duty cycle of 1.0 ms was still used, resulting from the analysis of the two elements of interest with dwell times of 0.3 ms and a settling of 0.2 ms. In the first experiment, single-shot measurements were performed at different locations on the SiC sample with an Al dopant level of 3×10^{19} cm^{-3} (~420 μg g^{-1}). The individually resolved SPRs of ^{27}Al and ^{29}Si can be seen in Fig. 5. Compared to the results of the NIST SRM 612, a longer washout time of 18 ms at FW0.01M was observed for SiC. This outcome could either reflect variations in the ablation behavior or differences in the overall analyte concentrations, resulting in changing peak widths.

The total crater depths were determined by profilometer measurements with a "DektakXT" (Bruker, MA, USA) as 2.2 μm (n = 40 shots). In an additional experiment, 5, 10, 20, 30, and 40 laser shots per position were fired onto the same samples, derived crater depth measurements showed a linear relationship between ablation depth and the applied number of laser shots, resulting in a mean ablation rate of 55 nm per shot, which is comparable to literature for ArF excimer-based lasers. The resulting ablation craters and a detailed graph of the ablation rate determination are shown in Fig. S1 and S2, respectively, in ESI 1.†[26]

A depth profile analysis of four Al-doped SiC samples was conducted using those parameters. The analysis of each sample included 30 different locations, with a gap of 5 μm between them. The depth profiles were conducted layer by layer, and a total of 40 layers were ablated in the process. In this way, depth profiles at thirty different locations on the sample could be recorded in *ca.* 120 s when using a frequency of 20 Hz. This time includes time for sample ablation and for transit of the laser between individual sample positions. The depth profiles of the analyzed samples can be seen in Fig. 6. For each ablation layer the thirty integrated peak areas were averaged to achieve a more representative measurement, represented by the standard deviation. The signal sequence of the LA-ICP-MS depth profiles correlates with the expected implantation profiles, as the upper 250 nm shows a roughly constant Al level, which decreases afterward. Moreover, it should be mentioned, that even lower implantation levels would be determinable, due to the enhanced signal-to-noise ratio of the short SPRs.

For a better assessment of the new LA-ICP-MS method for multi-element depth profiling, ToF-SIMS, a commonly used solid sampling technique for spatially resolved analysis, was used as a comparison.[20] Depth profiles of the same samples were conducted. In Fig. 6b, one can see the ^{27}Al signal normalized to ^{29}Si. The depth of the craters was measured using a stylus profilometer, "DektakXT" (Bruker, USA).

Upon initial observation, it is evident that the two techniques exhibit a strong level of agreement. However, for a more comprehensive comparison, a conversion of the normalized signal intensities into quantitative data is required. For this purpose, bulk online-LASIL measurements, as stated by Podsednik *et al.*,[27] were conducted. The online-LASIL measurement aimed to ablate the whole Al-doped region with a single ablation layer and to quantify the Al content of the ablated layer. A detailed description of the online-LASIL measurements is given in ESI 2† and a detailed description of the measurement parameters can be seen in Table S1.†

Obtained information about the total Al content (*cf.* ESI 2 Table S2†) allowed to calculate quantitative LA-ICP-MS and SIMS depth profiles through the alignment of ablation depths.

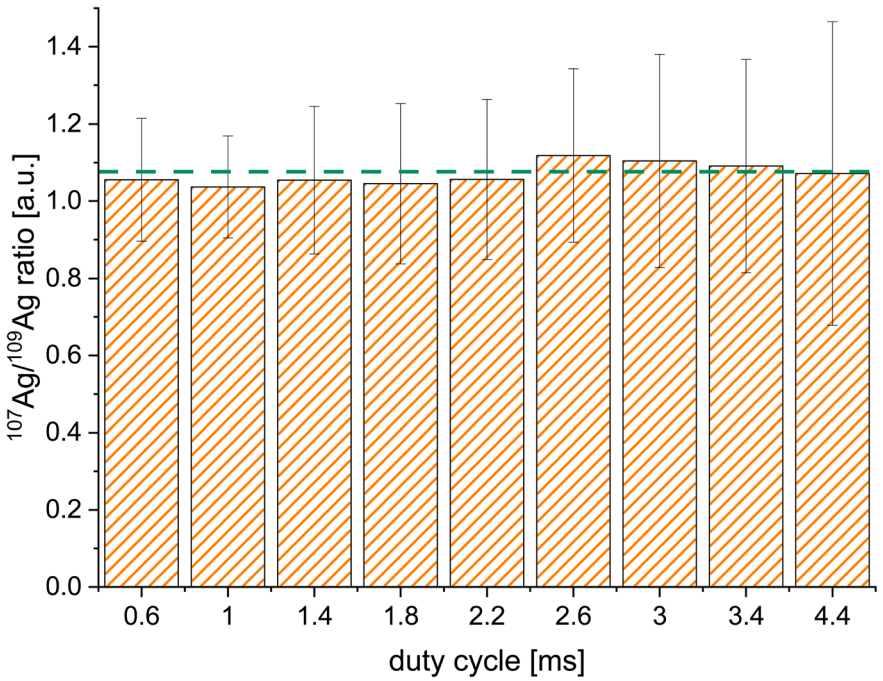

Fig. 4 Averaged $^{107}Ag/^{109}Ag$ ratio of the 30 SPRs with different duty cycles. The green dotted line depicts the naturally occurring $^{107}Ag/^{109}Ag$ ratio. The error bars represent the standard deviation of the 30 calculated $^{107}Ag/^{109}Ag$ ratios.

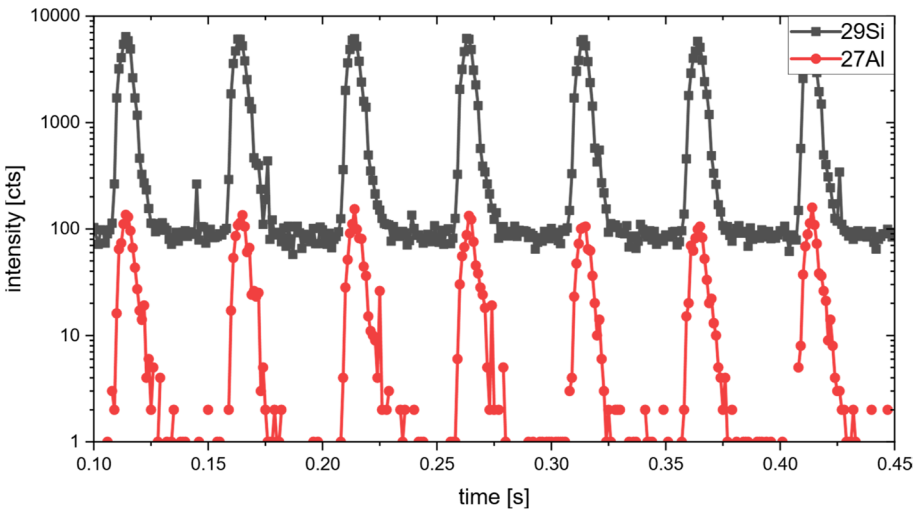

Fig. 5 SPRs of ^{27}Al and ^{29}Si using a duty cycle of 1.0 ms.

The calculated quantitative depth profiles for LA-ICP-MS and ToF-SIMS are illustrated in Fig. 7.

The quantitative depth profiles obtained from LA-ICP-MS and ToF-SIMS within the upper 250 nm constant doped region show excellent conformity with the targeted Al-atom density ranging from 1×10^{19} to 3×10^{20} atoms cm^{-3}. This indicates the success of the online-LASIL quantification approach and the accurate recording of the SPRs, since ^{27}Al is normalized to ^{29}Si for each signal.

When comparing the two techniques, it is crucial to emphasize the fast sampling speed of the proposed LA-ICP-MS approach. An area of 12 000 μm^2 is characterized in just 2 minutes, in stark contrast to the 30 minutes analysis period required by ToF-SIMS for a slightly smaller area of 10 000 μm^2. This enables the analysis of larger sample areas in the same or even lower times with LA-ICP-MS, a prerequisite for gaining more representative results. Thus, demonstrating the analytical power of utilizing SPRs for high-throughput applications. While ToF-SIMS provides for this sample material a better depth resolution of 6 nm compared to the 55 nm achieved with LA-ICP-MS, LA-ICP-MS can analyze deeper regions of the sample in a reasonable amount of time.

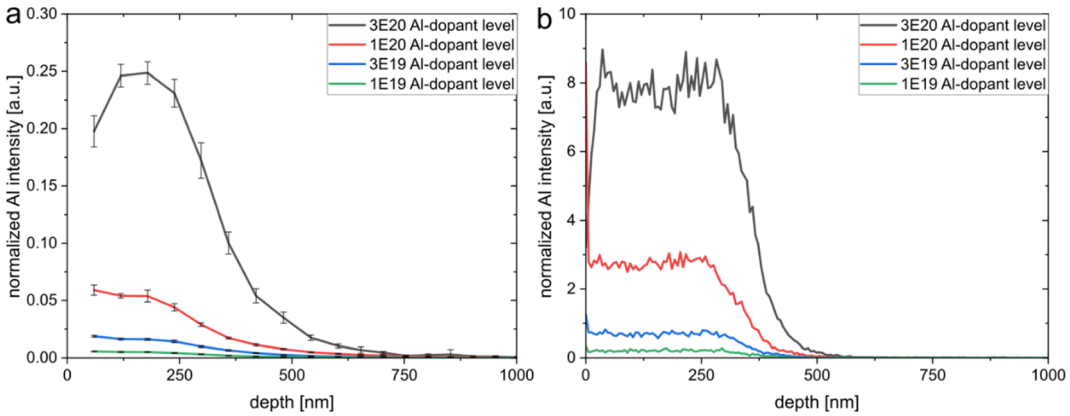

Fig. 6 (a): Qualitative depth profiles of different Al-doped SiC samples acquired with LA-ICP-MS using SPR, ^{27}Al-signal is normalized to ^{29}Si. The error bars represent the standard deviation of the 30 averaged peak areas of each ablation layer. (b): Qualitative depth profiles of Al-doped SiC samples acquired with ToF-SIMS, ^{27}Al signal is normalized to ^{29}Si.

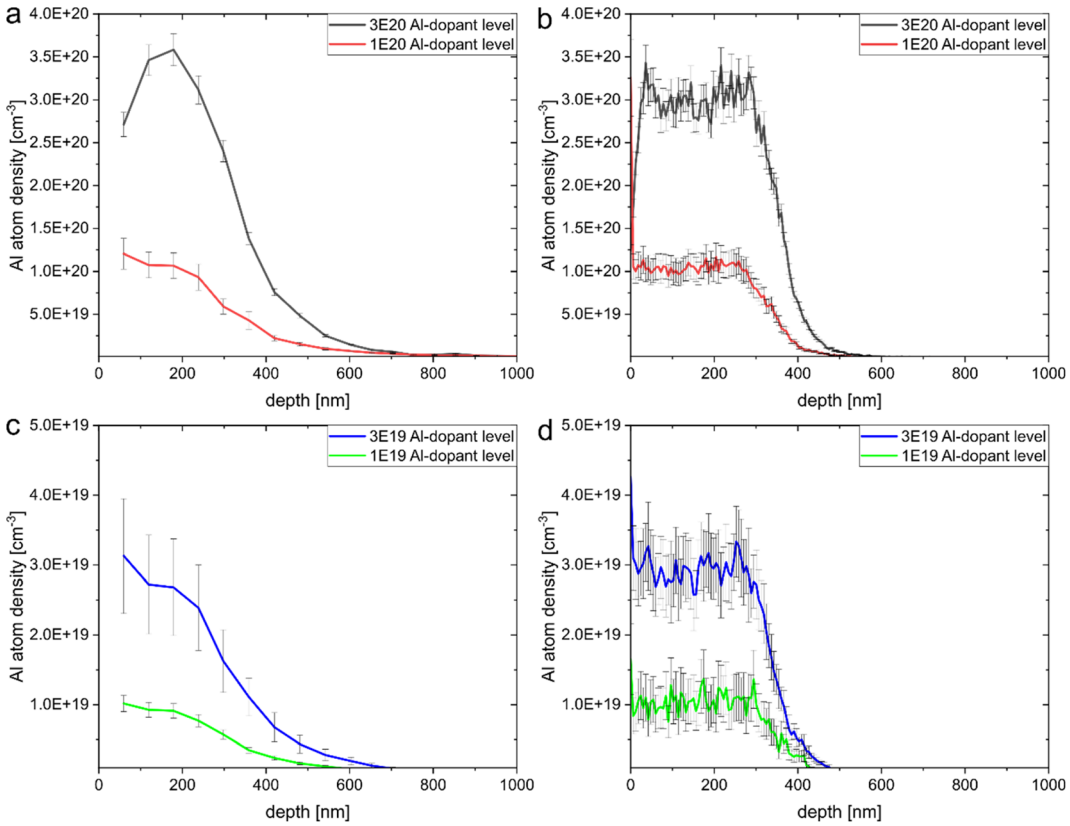

Fig. 7 (a and c): Quantitative LA-ICP-MS depth profiles of Al-doped SiC samples obtained with online-LASIL as a matrix-matched standard. (b and d): Quantitative ToF-SIMS depth profiles of Al-doped SiC samples obtained with online-LASIL as a matrix-matched standard. The error bars represent the fitting of multiple ($n = 5$) online-LASIL measurements into the qualitative depth profiles.

Examining the doped regions between 250 nm and 600 nm, the Al atom density in ToF-SIMS profiles declines more rapidly. This observation might be due to the difference in depth resolution and operating conditions between LA-ICP-MS and ToF-SIMS. However, considering the significant reduction in measurement time by a factor of fifteen and enhanced signal-to-noise ratios, LA-ICP-MS using short SPRs can still deliver competitive and more representative results.

4 Conclusion

This work introduces the implementation of short SPRs for the analysis of multiple elements in quadrupole detection systems. The optimization of the dwell time on the NIST SRM 612 demonstrated that besides the overall length of the dwell time, the integration ratio also impacts the deviation of the analysis of short SPRs. With the optimized duty cycle, the measured ratio

of ^{107}Ag and ^{109}Ag within a 10 ms FW0.01M SPR, with a deviation of 10%, was in good agreement with their natural abundance. This demonstrates that the speed of the data acquisition of the ICP-Q-MS is sufficient to use the data of each SPR.

To demonstrate the applicability of this method for novel high-performance materials, Al-doped SiC, a wide bandgap semiconductor heavily used for high-power applications, was analyzed. The LA-ICP-MS depth profile analysis demonstrates the improved signal-to-noise ratio of SPR, as even lower implantation levels would be determinable. Considering the obtained depth resolution of 55 nm, which is a remarkable result for LA-ICP-MS analysis, combined with high sampling speeds, the improvements of this approach become evident. Moreover, the comparison with ToF-SIMS showed good conformity with the LA-ICP-MS depth profiles. Those results demonstrate that using a quadrupole detection system, the measurement of SPRs with an 18 ms FW0.01M can be reliably recorded for two isotopes.

This work lays the foundation for multi-element analysis using a single pulse response with a quadrupole detector. Future work will focus on reducing settling times to enable the measurement of even more elements. In addition, this study has shown improvements in depth profiling, which could also lead to increased speed and depth resolution in imaging experiments.

Author contributions

Maximilian Podsednik: writing – original draft, visualization, validation, methodology, investigation, data curation, conceptualization. Florian Fahrnberger: methodology, conceptualization. David Ken Gibbs: methodology, conceptualization. Birgit Achleitner: methodology, conceptualization. Silvia Larisegger: supervision, project administration, funding acquisition. Michael Nelhiebel: resources, funding acquisition. Herbert Hutter: supervision, resources, conceptualization. Andreas Limbeck: validation, supervision, resources, project administration, funding acquisition, conceptualization.

Conflicts of interest

The authors declare that they have no conflicts of interest.

Acknowledgements

This work was funded by the Austrian Research Promotion Agency (FFG, Project No. 884573/898207/905107). The authors acknowledge TU Wien Bibliothek for financial support through its Open Access Funding Program. The authors thank Gregor Pobegen for the SiC samples responsible for the measurements.

References

1 M. Bonta, J. J. Gonzalez, C. D. Quarles, R. E. Russo, B. Hegedus and A. Limbeck, *J. Anal. At. Spectrom.*, 2016, **31**, 252–258.
2 S. Theiner, S. J. M. Van Malderen, T. Van Acker, A. Legin, B. K. Keppler, F. Vanhaecke and G. Koellensperger, *Anal. Chem.*, 2017, **89**, 12641–12645.
3 D. Chew, K. Drost, J. H. Marsh and J. A. Petrus, *Chem. Geol.*, 2021, **559**, 119917.
4 Y. S. Liu, Z. C. Hu, M. Li and S. Gao, *Chin. Sci. Bull.*, 2013, **58**, 3863–3878.
5 J. Willner, L. Brunnbauer, S. Larisegger, M. Nelhiebel, M. Marchetti-Deschmann and A. Limbeck, *Talanta*, 2023, **256**, 124305.
6 F. Horak, A. Nagl, K. Föttinger and A. Limbeck, *Microchim. Acta*, 2020, **187**, 641.
7 R. Russo, *Talanta*, 2002, **57**, 425–451.
8 B. Fernandez, F. Claverie, C. Pecheyran and O. F. X. Donard, *TrAC, Trends Anal. Chem.*, 2007, **26**, 951–966.
9 A. Limbeck, M. Bonta and W. Nischkauer, *J. Anal. At. Spectrom.*, 2017, **32**, 212–232.
10 J. S. Becker, A. Matusch and B. Wu, *Anal. Chim. Acta*, 2014, **835**, 1–18.
11 J. Pisonero, B. Fernandez and D. Gunther, *J. Anal. At. Spectrom.*, 2009, **24**, 1145–1160.
12 T. Van Acker, S. J. M. Van Malderen, T. Van Helden, C. Stremtan, M. Sala, J. T. van Elteren and F. Vanhaecke, *J. Anal. At. Spectrom.*, 2021, **36**, 1201–1209.
13 H. A. O. Wang, D. Grolimund, C. Giesen, C. N. Borca, J. R. H. Shaw-Stewart, B. Bodenmiller and D. Günther, *Anal. Chem.*, 2013, **85**, 10107–10116.
14 S. J. M. Van Malderen, J. T. van Elteren and F. Vanhaecke, *J. Anal. At. Spectrom.*, 2015, **30**, 119–125.
15 G. Craig, A. J. Managh, C. Stremtan, N. S. Lloyd and M. S. A. Horstwood, *Anal. Chem.*, 2018, **90**, 11564–11571.
16 A. Gundlach-Graham and D. Günther, *Anal. Bioanal. Chem.*, 2016, **408**, 2687–2695.
17 O. Laurent, M. Guillong, C. A. Heinrich, K. Neubauer and C. Stephan, *J. Anal. At. Spectrom.*, 2021, **36**, 2043–2050.
18 K. H. Chun, J. T. S. Lum and K. S. Y. Leung, *Anal. Chim. Acta*, 2022, **1192**, 339389.
19 M. Šala, V. S. Šelih, C. C. Stremtan, T. Tămaș and J. T. Van Elteren, *J. Anal. At. Spectrom.*, 2021, **36**, 75–79.
20 G. Friedbacher and H. Bubert, *Surface and Thin Film Analysis : a Compendium of Principles, Instrumentation, and Applications*, Wiley-VCH, Weinheim, 2nd edn, 2011.
21 M. V. Rao, *Solid-State Electron.*, 2003, **47**, 213–222.
22 F. Roccaforte, P. Fiorenza, M. Vivona, G. Greco and F. Giannazzo, *Materials*, 2021, **14**, 3923.
23 J. W. Zhou, H. T. Zhu, Q. C. Song, Z. W. Ding, J. Mao, Z. F. Ren and G. Chen, *Nat. Commun.*, 2022, **13**, 2482.
24 A. Hallen and M. Linnarsson, *Surf. Coat. Technol.*, 2016, **306**, 190–193.
25 V. Heera, D. Panknin and W. Skorupa, *Appl. Surf. Sci.*, 2001, **184**, 307–316.
26 L. I. L. Balcaen, J. Lenaerts, L. Moens and F. Vanhaecke, *J. Anal. At. Spectrom.*, 2005, **20**, 417–423.
27 M. Podsednik, M. Weiss, S. Larisegger, J. Frank, G. Pobegen, M. Nelhiebel and A. Limbeck, *Spectrochim. Acta, Part B*, 2023, **205**, 106705.